Materials Horizons

ROYAL SOCIETY OF CHEMISTRY

COMMUNICATION

View Article Online
View Journal | View Issue

Cite this: *Mater. Horiz.*, 2020, 7, 919

Received 23rd October 2019,
Accepted 5th December 2019

DOI: 10.1039/c9mh01688k

rsc.li/materials-horizons

Poly(ionic liquid) hydrogel-based anti-freezing ionic skin for a soft robotic gripper†

Ziyang Liu, ‡[a] Yue Wang,‡[b] Yongyuan Ren, [a] Guoqing Jin, [c] Chengcheng Zhang,[c] Wei Chen[d] and Feng Yan *[ac]

Capable of converting stimuli into electrical signals, hydrogel-based ionic devices are of great significance in soft robots, wearable devices, and artificial sensors. However, profound challenges remain in developing ionic devices that retain their properties in extreme environmental conditions, such as subzero temperatures. Based on a zwitterionic poly(ionic liquid) (PIL), an anti-freezing hydrogel was designed and synthesized for use in a multimodal artificial skin. This zwitterionic PIL hydrogel exhibited super-stretchability (approximately 900%), self-healing ability, and high conductivity (−1.1 S m^{-1}), even at low temperature (−20 °C). Based on this zwitterionic PIL hydrogel, three sensing modes, capacitive, resistive, and triboelectric modes, can be achieved in one device, which is stable under a wide temperature range (−20 °C to 60 °C). Further applications of these multimodal sensors with a soft robotic gripper suggested a new approach for developing sophisticated stimuli-responsive skin with multifunctionality and adaptability to varied environmental conditions.

New concepts

Most of the traditional hydrogel based artificial skins inevitably lose their self-healing ability, transparency, conductivity, and stretchability at sub-zero temperature because the aqueous solvent is frozen. Hence anti-freezing solvents (such as glycol, glycerol, sorbitol, or a mixture of them) have been widely applied to prevent the freezing of hydrogels at sub-zero temperatures. However, the conductivity and biocompatibility of the cryoprotectant solution-based hydrogels need to be improved, especially at low temperatures. In this work, zwitterionic poly(ionic liquid) (PIL), with equal positively charged and negatively charged groups in one unit, has been used for the preparation of hydrogels. The prepared poly(ionic liquid) hydrogel (PIL gel) showed super-stretchability (~900%), self-healing ability, and high conductivity (1.1 S m^{-1}) even at −20 °C. To further investigate the antifreeze mechanism of PIL gel, molecular dynamics simulations (MD) were also conducted. The PIL gel based ionic-skin with three modes, including capacitive, resistive and triboelectric sensing modes, can be easily switched simultaneously in one device with simple sandwiched structures. Combined with a soft robotic gripper, the multimodal PIL-Skin makes the gripper suitable for a variety of application environments. We expect that our work may provide a platform for further sophisticated stimuli-responsive skin design and development.

Introduction

As the largest organ of human bodies, skin can perceive multiple external stimuli and convert them into physiological signals for neural recognition.[1] With the continuing development of artificial intelligence,[2,3] soft robotics,[4,5] and wearable devices,[6,7] artificial skin-like materials promise to be an important medium for human-machine interaction,[8] and such materials have gained a great deal of industrial and academic attention. During the last decade, electronic skin based on specific sensors in dielectric materials has been proposed to emulate responses of natural skin to external stimuli.[9,10] In nature, ions represent a unique basis for biological activities, including effective neural sensing signal generation and transduction. Hydrogels are a class of advanced materials that can provide space for ion diffusion transfer and have demonstrated many advantages of independent ionic conductivity, biocompatibility, optical transparency, self-healing capability, and stretchability,[11] which have been widely used in flexible electronics and bionic devices, such as sensors and conductors.[12] Using two polyacrylamide (PAAm) hydrogel layers and a dielectric layer, Suo and co-workers developed the first generation of "ionic skin," which could record pressure and strain.[13] Wu *et al.* prepared a self-healable ionic skin by using a bioinspired supramolecular hydrogel, which also achieved multiple sensitivity.[14] Combining electrostatic induction with

[a] *Department of Polymer Science and Engineering, College of Chemistry, Chemical Engineering and Materials Science, Soochow University, Suzhou 215123, China. E-mail: fyan@suda.edu.cn*
[b] *Department of Electrical and Computer Engineering, University of Illinois at Urbana-Champaign, Urbana, Illinois 61801, USA*
[c] *Robotics and Microsystems Centre, School of Mechanical and Electric Engineering, Soochow University, Suzhou 215123, China*
[d] *Research Centre for Smart Wearable Technology, Institute of Textiles and Clothing, The Hong Kong Polytechnic University, Hong Kong 999077, P. R. China*
† Electronic supplementary information (ESI) available. See DOI: 10.1039/c9mh01688k
‡ Authors with equal contributions.

triboelectrification effects, triboelectric nanogenerators (TENG) based on an ionic hydrogel reported by Wang have also been widely studied as an energy collector and passive sensor for self-powered devices.[15,16]

However, most of the traditional hydrogels inevitably lose their self-healability, transparency, conductivity, and stretchability at sub-zero temperature because the aqueous solvent is frozen, which thus hinders their practical applications at low temperatures.[17] Hence anti-freezing solvents (such as glycol, glycerol, sorbitol, or a mixture of them) have been widely applied to prevent the freezing of hydrogels at sub-zero temperatures.[18,19] However, the conductivity and biocompatibility of the cryoprotectant solution-based hydrogels usually need to be improved, especially at low temperatures. Relatively low conductivity of these anti-freezing hydrogels limits their practical applications in electrochemical devices.

Recently, intensive attention has been paid to the poly(ionic liquids)[20] (PILs, polymers formed from IL monomers), because they combine properties of ionic liquid (ILs), such as low volatility as well as thermal and electrochemical stabilities, with the mechanical durability properties of polymers.[21,22] Zwitterionic poly(ionic liquids), with equal positively charged and negatively charged groups in one unit, have been widely used 0as biocompatible materials,[23,24] and anti-fouling and anti-frost coatings mainly because of their strong hydration effect.[25,26] In this work, based on a zwitterionic poly(ionic liquid), a hydrogel (PIL gel) retained super-stretchability (~900%), self-healing ability, and high conductivity (1.1 S m^{-1}) even at low temperature (−20 °C). Depending on the PIL gel, a multimodal artificial skin was fabricated and characterized. The PIL-Skin can function in parallel in three modes: capacitive, resistive, and triboelectric modes. In capacitive mode, this PIL-Skin can detect pressure in the range of 1.1 to 45 kPa. In resistive mode, both temperature (−20 °C to 60 °C) and strain (0 to 160%) can be sensed. Furthermore, integration of a TENG with this resistive mode enables the PIL-Skin to perceive not only temperature and strain but also active pressure (0.5 to 40 kPa) at −20 °C, simultaneously. The device also achieved superior stretchability and autonomous self-healing ability. We expect that our work may provide a platform for further sophisticated stimuli-responsive skin design and development.

Results and discussion

Fig. 1A shows the chemical structure of the PIL gel, prepared *via* free-radical copolymerization of a zwitterionic IL monomer, 1-vinyl-3-(carboxymethyl)-imidazolium, and acrylamide (AAm) in KCl aqueous solution. The chemical structure and purity of this PIL gel were characterized by Fourier transform

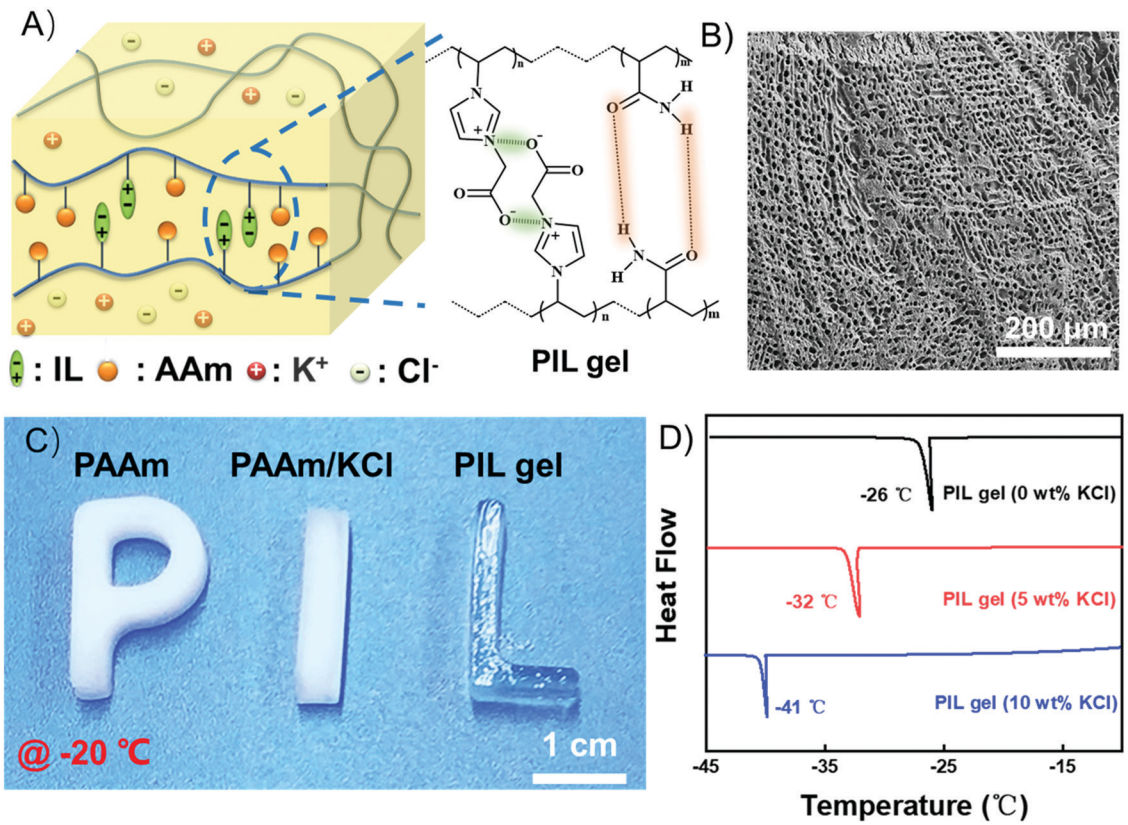

Fig. 1 Structure and anti-freezing characterization of the PIL gel. (A) Chemical structure of the zwitterionic PIL gel; (B) scanning electron microscopy (SEM) image of the freeze-dried PIL gel; (C) digital photos of the polyacrylamide (PAAM), PAAM/KCl (KCl, 12 wt%), and zwitterionic PIL hydrogel (KCl, 10 wt%) stored at −20 °C for 1 h; (D) differential scanning calorimetry (DSC) tests of the PIL gels containing different amounts of KCl.

infrared (FT-IR) spectroscopy.[27] Compared with PIL gel, the C═O stretching bands of AAm (1668 cm^{-1}) and IL (1625 cm^{-1}) shift to approximately 1696 cm^{-1}. The corresponding peaks of N–H shifted from 1610 cm^{-1} to 1556 cm^{-1}. The results indicate the formation of hydrogen bonds between the C═O and N–H groups. Compared with the PIL, the corresponding peaks of imidazolium groups shifted from 1407 cm^{-1} to 1357 cm^{-1}, suggesting the ionic associations between the imidazolium and $–COO^-$ groups (Fig. S1, ESI†). Fig. 1B shows a scanning electron microscopy (SEM) image of the freeze-dried PIL gel. The interconnected porous architecture promises ion transport that is similar to previous reports.[11] This gel can be easily cut into any desired size and shape and exhibits high transparency (approximately 92% in visible light, Fig. S2, ESI†). Fig. 1C and Video S1 (ESI†) demonstrated the anti-freezing performance comparison among the polyacrylamide (PAAM), PAAM/KCl, and zwitterionic PIL gels. These hydrogels were cut into desired shapes and stored at −20 °C for 1 h. Both PAAm and PAAm/KCl hydrogels changed from transparent to opaque and fragile quickly, while the PIL gels kept transparent and flexible, suggesting that no crystallization of water occurred in our PIL gels. To further explore the freeze-tolerant ability of our PIL gel, differential scanning calorimetry (DSC) tests of the samples were conducted (Fig. S3, ESI†). It can be seen that the PAAm hydrogel shows a freezing point at approximately −3 °C, which is similar to the results reported. It has already been demonstrated that the addition of inorganic salts could bring down the freezing point of the water because of the colligative property.[28,29] Compared with PAAm gel, the endothermic peak of the PAAm/KCl was further decreased to −14 °C. It should be noted that the PIL gel (without KCl) synthesized in this work showed a freezing point up to −26 °C, indicating the anti-freezing characteristic of the zwitterionic PIL. With the addition of KCl, the freezing point of the PIL gels shifts to −32 °C (KCl, 5 wt%) and −41 °C (KCl, 10 wt%) (Fig. 1D). However, further addition of KCl will induce salt precipitation.[14]

In nature, the freezing tolerance of biology is mainly attributed to biomacromolecules, such as antifreeze-proteins and antifreeze-glycoproteins.[30] These biomacromolecules are believed to be able to adhere to the ice surfaces.[31] Previous work has shown that polyampholytes which mimic biomacromolecules also have a good ice recrystallization inhibition activity, mainly because the water molecules can be tightly bound to the zwitterionic groups due to charge–dipole and dipole–dipole interactions.[32,33] For this PIL gel, the imidazole cation and the carboxylate anion formed a zwitterionic unit, guaranteeing strong water absorption capacity and water retention ability. Carboxylate has been used in anti-frog and anti-frost materials. It has also been shown that imidazolium-based gels can sequester in a non-freezable state up to 30% water by weight.[34] Therefore, both the hydrophilic group and the dipole moments of this zwitterionic IL unit provided the anti-freezing ability of our gel. To further investigate the antifreeze mechanism of PIL gel, molecular dynamics simulations (MD) were conducted.[35] Here, we investigated a 12-residue PAAm-ZIL (10 : 2) oligomer in an aqueous solution at 258 K, while a 12-residue PAAm chain was calculated for comparison (Fig. 2A). The diffusion property of water molecules has firstly been analysed. Mean square displacement (MSD) shows a linear relationship with the increase of simulation steps (Fig. S4a, ESI†). The slope of water molecules in the PAAm-ZIL system is lower than it in the PAAm system, indicating that the PIL system has a stronger binding effect on water molecules.[36,37] To compare the binding capacity of the two polymer chains with water molecules, the potential of mean force (PMF) was adopted to represent the energy barrier effect of the hydration layer of the polymer chains (Fig. 2B). The first minimum point on the potential energy is the contact minimum (CM), which is the distance between the polymer chain and a water molecule. The second minimum point on the potential energy curve is the solvent separation minimum point (SSM), which is the position where the second solvent layer contacts with water molecules. It can be seen that there is a relatively high barrier between CM and SSM, namely the barrier of the solvent layer (BS), representing the solvent layer barrier that needs to be overcome when water molecules enter the first hydration layer from the second hydration layer of the polymer chain. The binding energy (ΔE^+) between the polymer and water molecule depends on SSM and BS ($\Delta E^+ = E_{BS} - E_{SSM}$). The binding energy ($\Delta E^+$) between the PIL chain and water molecules (4.91 kJ mol^{-1}) is lower than that of a PAAm chain (6.12 kJ mol^{-1}), indicating that the binding of water molecules to the PIL is relatively more straightforward. The dissociation energy (ΔE^-) depends on CM and BS ($\Delta E^- = E_{BS} - E_{CM}$). Compared with the PAAm chain (2.32 kJ mol^{-1}), the dissociation energy between the PIL chain and water molecules (4.38 kJ mol^{-1}) is higher, indicating that the water molecules are more laborious to dissociate with PAAm-ZIL than the PAAm chain, which is consistent with the trend of MSD. The relaxation time of water molecules can indicate the binding condition of the polymer membrane to water molecules, especially for the zwitterionic polymer. Therefore, the dipole autocorrelation function was used to analyze the dipole relaxation time.[38] As shown in Figure S4b, water molecules surrounding the PAAm-ZIL chain have a longer dipole relaxation time, which indicates that the PAAm-ZIL chain can well stabilize the oscillation of water molecules. Because the dipole direction of the water molecule can only oscillate slightly near the equilibrium position, the icing process was significantly slowed.

The mechanical property of the PIL gel was further tested at both 20 °C and −20 °C, respectively. According to the rheological test, The G' and G'' of PIL gel on a temperature sweep from 20 to −60 °C can be seen in Fig. 2C. When the temperature decreased to −20 °C, the G' of the PIL gel only had a slight rise, which indicates a stable elasticity of the PIL gel at sub-zero temperatures. In contrast, as the temperature goes up to 60 °C, the G' and G'' shows a slight decline.[39] Corresponding to the rheology test, the uniaxial stretching of the PIL gel can be extended to ∼1050% at 20 °C. The stretchability of the PIL gel was slightly decreased to ∼900% at −20 °C, probably due to the limitation of polymer chain motions at low temperatures. And the stretchability shows a small increase at 60 °C, mainly because of the enhancement of the chain motions (Fig. 2D and Video S2, ESI†). Fig. 2E shows the conductivity of the PIL

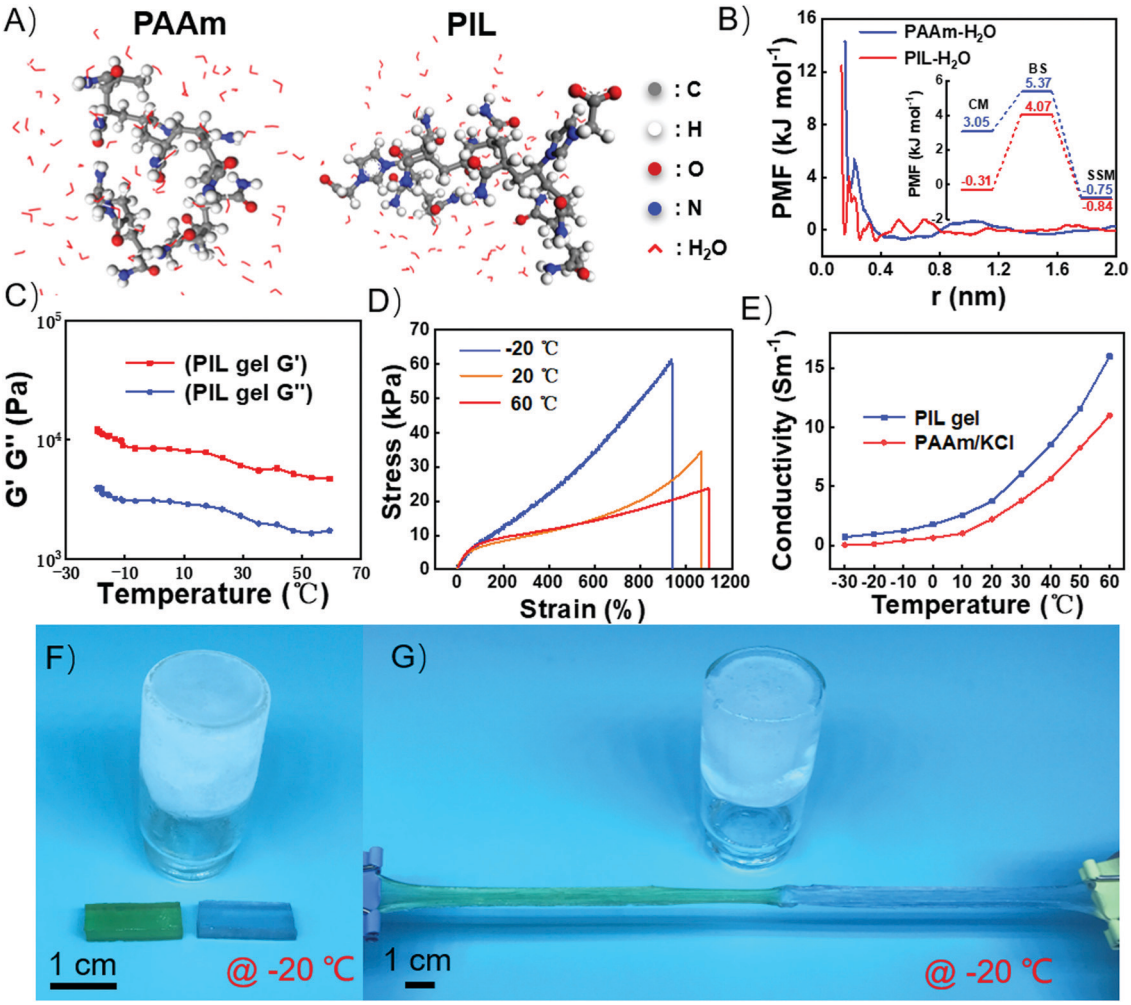

Fig. 2 (A) Chemical structures of PAAm and PAAm-ZIL chains in water; (B) potential of mean force (PMF) between the polymer chains and water molecules; the inset on the right contains only maximum and minimum points of energy for clarity; (C) G' and G'' of the PIL gel on a temperature sweep at a constant shear strain (g) of 0.5% and a frequency (w) of 0.1 rad^{-1}; (D) uniaxial tensile test of the zwitterionic PIL gel at −20 °C and 20 °C; (E) conductivity digital comparison between zwitterionic PIL gel and PAAm gel under various temperatures; (F) photo of the cut PIL gels at −20 °C; (G) the self-healed gel can be stretched at −20 °C.

gel and PAAm gel under various temperatures. Compared with the PAAm (10% wt KCl) gel (4.1 S m^{-1}), this PIL gel exhibited a higher ionic conductivity (6.2 S m^{-1}) at −30 °C, because both the cationic and anionic counterions of polyzwitterions can provide preferential ion migration channels. The PIL gel still maintains high conductivity (approximately 0.8 S m^{-1}) at 30 °C, while the PAAm gel almost loses the ionic conductivity. As the temperature goes up to 60 °C, both of the two gels exhibit an obvious improvement in conductivity. It is assumed that ionic bonds between the zwitterionic IL moieties and hydrogen bonds between acrylamide groups can form cross-links within the polymer side-chains.[14] These ionic bonds and the hydrogen bonds form reversibly, making this PIL gel self-healable.[40] Fig. 2F and G show this self-healing ability. It can be seen that a cut PIL gel can be healed within 6 hours at −20 °C.

Fig. S5a (ESI†) schematically illustrates the structure of the PIL-Skin. Here, the commercially available Very High Bond (VHB 4905, 3M) tapes, with excellent stretchability, high transparency, and self-healing ability,[41,42] were applied as a dielectric material. This fabricated device also exhibited an excellent stretchability (~710%) (Fig. S5b, ESI†). Two pieces of PIL gel (20 mm × 20 mm × 0.5 mm) were sandwiched by three pieces of VHB tape (30 mm × 30 mm × 0.5 mm). An essential characteristic of human skin is autonomous recovery after being damaged. Here, the PIL-Skin showed self-healing capability like human skin because both the VHB and PIL gel are self-healable. As shown in Fig. S5d (ESI†), this PIL-Skin serves as a conductor to light up a red LED (light-emitting diode). When the PIL-Skin was severed into two pieces, the LED light-piping extinguished immediately. Once two pieces were brought back together, light conduction was restored, and the LED indicator functioned again. Thus, this repaired PIL-Skin exhibited superior transparency, stretchability, and self-healing capability. To further demonstrate the applications of the PIL-Skin, a soft robotic gripper attached with the PIL-Skin was applied in this work, as can be seen in Fig. S5e (ESI†).

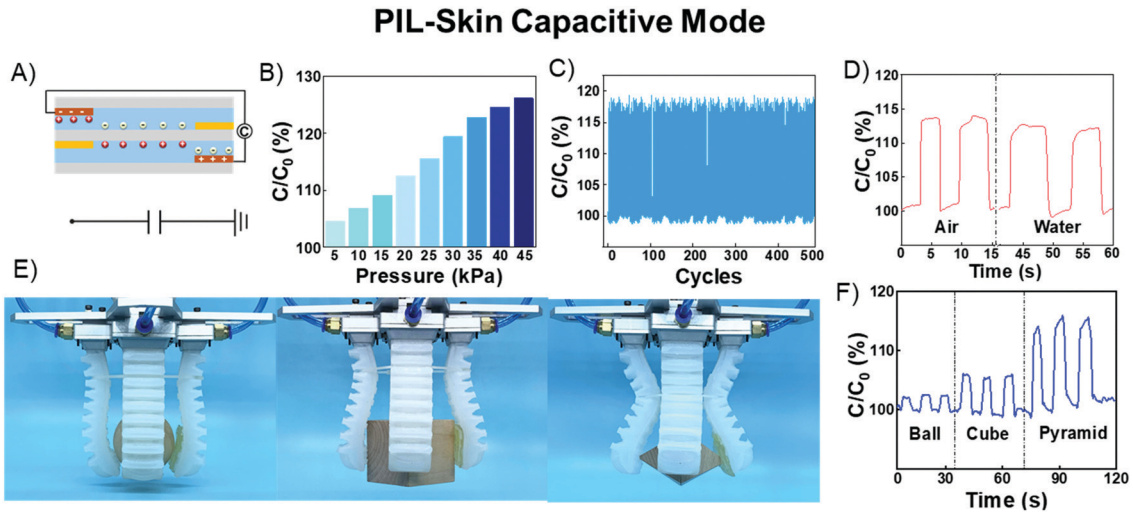

Fig. 3 (A) PIL-Skin in capacitive mode; (B) capacitive signals under various pressures at room temperature; (C) under 500 cycles and (D) in air and water; (E) digital photo of a soft robotic gripper attached with a PIL-Skin holding a woodware (ball, square or pyramid); (F) variation of capacitive signal during the interaction.

It is known that capacitive sensors have simple device structures, high sensitivity, and exhibit long-term stability even when temperature and humidity are variable.[43,44] The working principle of PIL-Skin in capacitive mode can be seen in Fig. 3A. In this mode, two conductive PIL gels and a dielectric layer (VHB) compose a parallel plate capacitor. When extensional forces are applied to this device, the expanded area of PIL-Skin will lead to an increase in capacitance, which can be used to detect pressure. Fig. 3B illustrates capacitive variation under different pressures at room temperature. This PIL-Skin in the capacitive mode has a range of 1.1 kPa to 45.2 kPa for pressure detecting. The sensitivity (S_C) is defined as $S_C = (\Delta C/C_0)/\Delta P$, where ΔC is the relative change of the capacitance, C_0 is the original capacitance and ΔP is the relative change of touch pressure. Upon a pressure lower than 45.2 kPa, the PIL-Skin shows a pressure sensitivity of 0.57% kPa^{-1}. When the pressure was beyond 45 kPa, the thickness of the device barely changed. Fig. 3C shows the capacitive signal with 500 cycles. A nearly constant response with little variance was observed, indicating the stability of the PIL-Skin. For TENG-based pressure sensors, water molecules in a dielectric effectively neutralize the surface electrostatic charges, resulting in an output reduction of the film TENG.[16] However, capacitive sensors are only slightly affected by water. PIL-Skin with both dry and damp surfaces was compared, proving that PIL-Skin in capacitive mode has excellent stability in both water and air (Fig. 3D). Fig. 3E shows the gripper holding a wooden ball, square, and pyramid, respectively. Because the inflation pressure of the gripper was constant (50 kPa), the contact pressure depended on the contact area of each woodware. As shown in Fig. 3F, the capacitive signals increased with the decrease of the contact area.

Dynamically physically cross-linked hydrogels have been used as strain sensors and temperature sensors, mainly because of their excellent stretchability and negative temperature change, coefficient (NTC) behavior.[45] In resistive mode, two PIL gels acted as strain resistance and thermistor, respectively (Fig. 4A). The stretched hydrogel usually has an apparent volume resulting in a variation of ion migration, and reflected in a change of resistance. The thermo-responsive resistivity of a hydrogel relies on its ionic conductivity, which varies with temperature. Ionic mobility increases with rising temperature. Furthermore, ion dissociation accelerates at high temperature and also contributes to an increasing concentration of charge carriers. Both effects contribute to the change in resistance at varied temperatures.

Temperature sensing properties of the PIL-Skin were observed by monitoring resistance variation with a heating platform and a refrigerator. It can be seen from Fig. 4B that the resistance of the device decreased monotonically with increasing temperature. Owing to low-temperature freezing-tolerance of this PIL gel, this device can work well even at −20 °C. While the temperature continues to fall, the resistance rises dramatically. The definition of sensitivity is similar to that in the capacitive mode while the original resistance is defined as the resistance at 25 °C. The sensitivity (S_T) is 11.3% $°C^{-1}$ at relatively low temperatures (−20 °C to 25 °C) and 2.1% $°C^{-1}$ at 25 °C to 60 °C. The temperature sensing repeatability of this device was further examined by continuous heating and cooling from −25 °C to 60 °C. A nearly constant response with little standard deviation was observed over 50 cycles (Fig. 4C). Such a stable conductivity of the PIL-Skin is probably due to the protection provided by the VHB, which eliminates water evaporation from the PIL gel. To further characterize the protection of the VHB, the weight variation of the PIL gel and VHB packaged PIL-Skin was recorded, simultaneously. The PIL gel lost water quickly in the first 3 days (32.4% loss) at room temperature with the average relative humidity (RH) of ~20% (Fig. S6a, ESI†). Such a dehydration could be greatly alleviated when the PIL gel is sealed with VHB tapes. For example, the weight retention of 96.9% was obtained even after 10 days

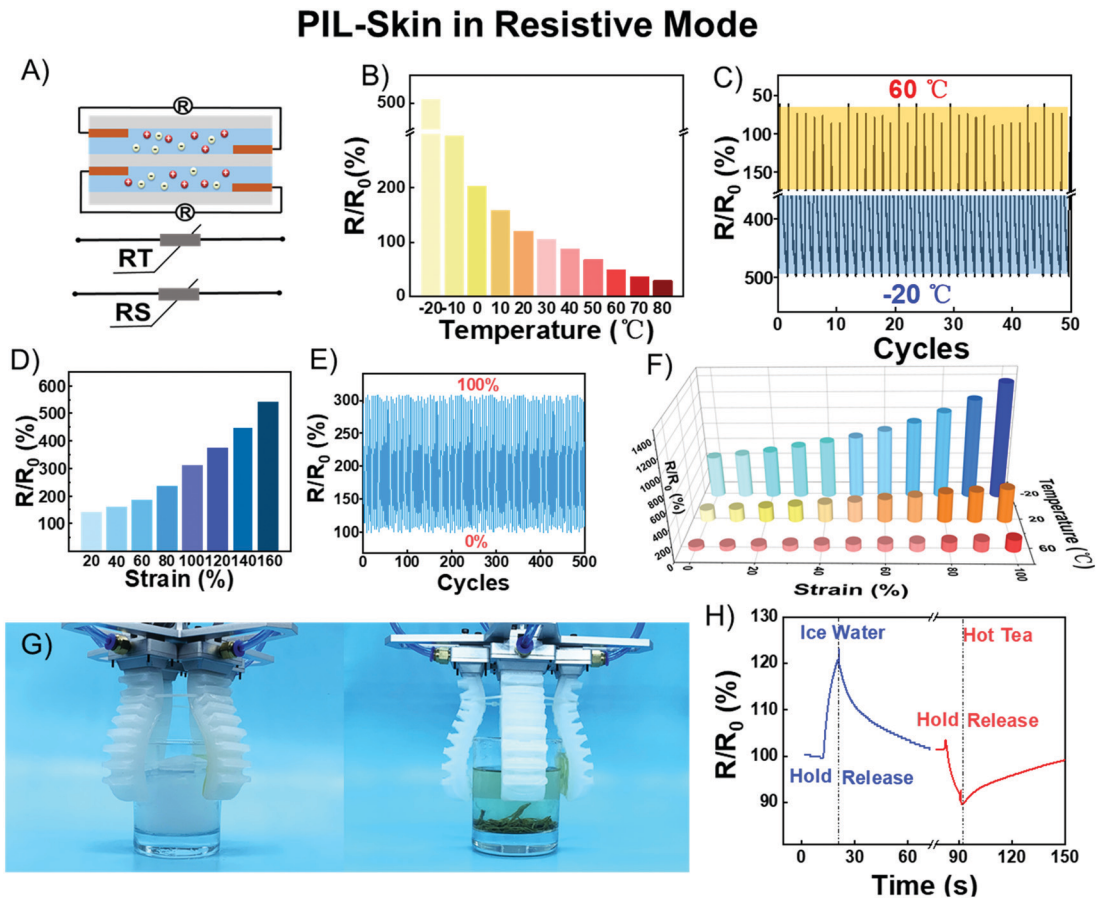

Fig. 4 (A) PIL-Skin in resistive mode; (B) resistances at varied temperatures; (C) dynamic responses of the thermistor to 50 cycles of heating and cooling between −20 °C and 60 °C; (D) resistance under variation in strain; (E) dynamic responses of the strain from 0 to 100% with 500 cycles; (F) resistive signals of the PIL skin upon the mutual effect of the varied temperature and strain; (G) photos of the soft gripper holding a cup of ice water and a hot tea (approximately 60 °C); (H) the resistive signal of the holding process.

under the same experimental conditions. The weight of PIL gel decreased to 58% at 60 °C for 3 h, while the PIL-Skin showed a relatively higher water retention ability (Fig. S6b, ESI†).

The resistance of the PIL-Skin increases monotonically with increasing strain to 160% strain (see Fig. 4D). The sensitivity S_S is 2.7% per %. The stretched hydrogel usually has an apparent volume change, resulting in a variation of ion migration, which is reflected in the change of resistance. A nearly constant response with little variance was observed over 500 cycles (Fig. 4E). Fig. 4F shows the resistance signals of the PIL Skin upon combined actions of temperature and strain. The *X*-axis, *Y*-axis, and *Z*-axis are strain, temperature, and the variation of resistance, respectively. Both the temperature reduction and the stretching increased the resistance of PIL Skin. Compared with room temperature and 60 °C, the resistance changes more dramatically with stretching at low temperature. Fig. 4G shows the gripper holding the ice water and hot tea, respectively (each holding process is 10 seconds). It can be seen that the resistance rose quickly upon holding the ice water, while it was reduced with the hot tea (Fig. 4H), indicating the temperature sensing ability of the PIL-Skin.[46]

As a device for collecting mechanical energy, the output of a TENG was also applied to pressure-sensitive devices.[47,48] Compared with capacitive sensors, triboelectric sensors show more advantages in perceiving dynamic stimuli and better temperature stability.[49] As shown in Fig. 5A, a single-electrode triboelectric nanogenerator which can detect pressure was fabricated using a grounded PIL gel. Another conducting PIL gel served as a resistance. The two working units do not interfere with each other; therefore, the PIL-Skin in this mode can sense pressure, temperature, and strain. Fig. S7 (ESI†) shows the working mechanism of a single electrode TENG.[50] This working mechanism of a TENG is based on the cooperation of triboelectric electrification and electrostatic induction. An open-circuit voltage was recorded by pressing a nylon film onto a PIL-Skin with different pressures (Fig. 5B). The resulting voltage increases linearly with pressure when this touch pressure is low and saturates after this pressure exceeds 39.8 kPa. The sensitivity (S_T) is defined as $S_T = \Delta V/\Delta P$, where ΔV is the relative change of the output voltage, and ΔP is the relative change of touch pressure. In the low-pressure region (<15 kPa), the PIL-Skin shows a relatively high-pressure sensitivity of 1.8 V kPa^{-1}. In the second region (15–40 kPa), this sensitivity decreases to 0.13 V kPa^{-1}. Fig. 5C shows the voltage output of the triboelectric mode at various temperatures. With the temperature increased

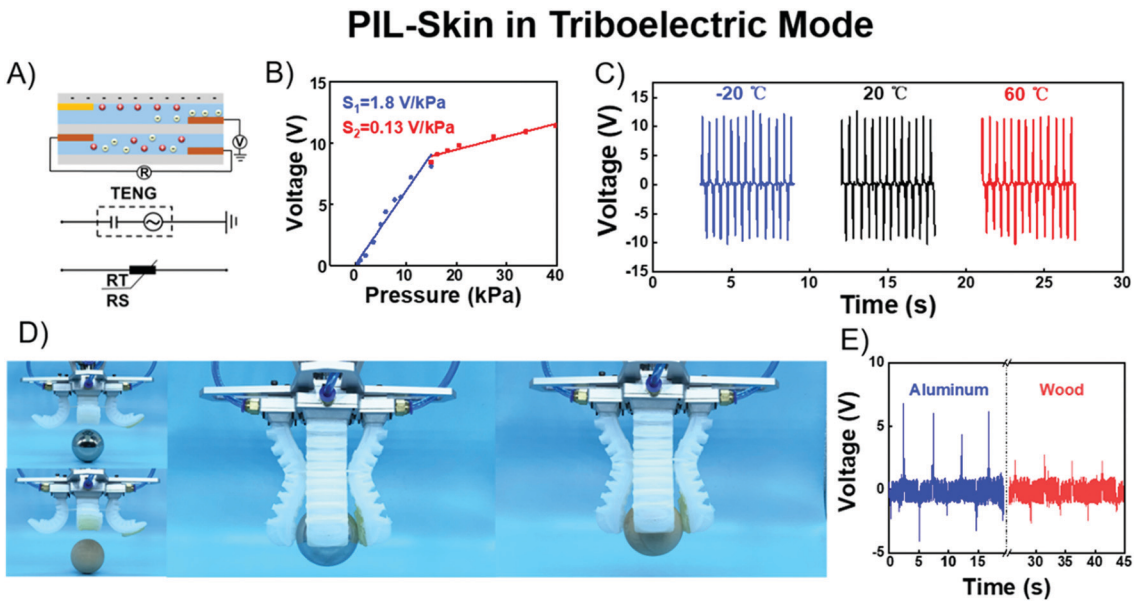

Fig. 5 (A) PIL-Skin in triboelectric mode: (B) the voltage signals of the PIL-Skin under various pressures; (C) voltage output from the PIL-Skin under 2 Hz blunt impacts (by 3 cm^2 PET ram) at −20 °C, 20 °C and 60 °C; (D) photos of the soft gripper holding an aluminium ball and a wooden ball; (E) voltage output during the holding process.

from −20 °C to 60 °C, the voltage kept constant, indicating the high stability of the triboelectric mode under various temperatures. Fig. 5D exhibits the holding process with the same exploration pressure (50 kPa) of the balls made of wood and aluminium, respectively. Because the triboelectric coefficient of aluminium is higher than that of wood, the voltage output of contacting the aluminium ball is higher. According to the triboelectric property of PIL-Skin, the soft robotic gripper can distinguish materials with various temperatures and surface roughness.

Conclusions

In summary, based on the synthesized anti-freezing zwitterionic PIL gel, a multimodal artificial skin, PIL-Skin, was fabricated for the application of soft robots. As an ion carrier, this dynamically crosslinked PIL gel provides not only excellent stretchability and self-healability but also a highly favourable low-temperature resistance to freezing, making the ionic device workable at low-temperatures and ultimate tensions. Based on the PIL gel, a multimodal PIL-Skin was designed and fabricated. The pioneering combination of capacitive sensing, thermistor performance, and triboelectric effects in one device means that PIL-Skins possess the ability to sense multiple signals in complex situations. Combined with a soft robotic gripper, the multimodal PIL-Skin makes the gripper suitable for a variety of application environments. Thus, a practical sensor for artificial skin has been demonstrated. Furthermore, strategies for designing and fabricating skin-like sensors exemplified here may promote the development of next-generation intelligent skin-like devices.

Experimental section

Materials

Vinyl imidazole, methyl chloroacetate, KOH, KCl, acrylamide (AAm), *N*,*N*,*N*′,*N*′-tetramethyl ethylenediamine (TEMED), and ammonium persulfate (APS) *N*,*N*-methylenebisacrylamide (MBAA) were all from Sigma-Aldrich. VHB film (3M VHB 4905) was used as a dielectric elastomer film.

Synthesis of PIL gel

The PIL gel was fabricated by free-radical copolymerization of 1-vinyl-3-(carboxymethyl)-imidazole (zwitterionic IL) and acrylamide (AAm). Precursor solution was obtained by dissolving AAm (5 mmol, 0.35 g), ZIL (1 mmol, 0.15 g) and KCl (0.2 mmol, 0.14 g) into deionized water (4 mmol, 0.72 g). Then, APS 1 wt% and TEMDA 1 wt% with respect to the weight of the precursor solution were added as an initiator and catalyser, respectively. The gel was cured at room temperature for 30 min. The thickness and shape of the gel can be controlled by a mold.

Preparing a polyacrylamide hydrogel as a contrast

The polyacrylamide hydrogels were prepared like the PIL gel. AAm (5 mmol, 0.35 g) and KCl (0.2 mmol, 0.15 g) were dissolved into deionized water (4 mmol, 0.72 g). Subsequently, initiator (APS 1 weight%), catalyser (TEMDA 1 weight%) and MBAA (0.2 weight%) were added in. The mixture was then transferred into a tetrafluoroethylene mold for 30 min.

Fabrication of the PIL-Skin

Three VHB tapes (3M VHB 4905, 500 mm thick) were used as substrates. Aluminium chips (20 mm × 2 mm) were applied at the interfaces for mode conversion, and fixed the size of the PIL

gels (20 mm × 20 mm × 0.5 mm) and VHB (30 mm × 30 mm × 0.5 mm). The effective contact area between the Al chips and PIL gel was about 2 mm2 (see Fig. S5c, ESI†).

Characterization of the PIL gel

The resistance of the gel was recorded by an AUTOLAB PGSTAT 302N. The gel was encapsulated in a stainless-steel mold for Electrochemical Impedance Spectroscopy (EIS) tests. The rheological behavior was investigated by a RheoWin MARS 40 modular advanced rheometer using a 25 mm parallel plate. The differential scanning calorimetry was tested by PerkinElmer DSC 4000. The mechanical tests were conducted by an Instron 5900 system. The gel was put in the environmental chamber of the Instron 5900 with a set temperature for 10 min before the tensile test. The scanning electron microscope (SEM) tests were conducted by a Hitachi S-4700. The SEM images were obtained by liquid nitrogen quenching and freeze-drying of the gel.

Characterization of the PIL gel based PIL-Skin

The thickness of VHB tape and the whole device was measured by using a screw gauge. The resistive and capacitive signals were recorded by using an LCR meter (TH2830). The output voltage from the TENG was measured by an oscilloscope (Tektronix, MDO 3014). The mechanical pressure and stretch test were executed by an Instron 5900 system.

Molecular dynamics

The 12-residue polymer chain with 80 water molecular was built by the Amorphous Cell of Materials Studio 8. Energy minimization was carried out by the Forcite module of MS software under a compass II force field. First, molecular dynamics simulation was conducted at 298 K temperature with at least 10 ns, and the balance of the system was determined by energy fluctuation and mean square displacement of water molecules. Then, molecular dynamics simulation was conducted with 5 ns, in which the simulation step length was 2 fs, and the track information was recorded at an interval of 0.2 ps for subsequent analysis.

Conflicts of interest

There are no conflicts to declare.

Acknowledgements

This work was supported by the National Natural Science Foundation for Distinguished Young Scholars (21425417), the National Natural Science Foundation of China (21835005 and U1862109), and by the Priority Academic Program Development of Jiangsu Higher Education Institutions.

Notes and references

1 H. Yuk, B. Lu and X. Zhao, *Chem. Soc. Rev.*, 2019, **48**, 1642–1667.
2 K. Li, Y. Shao, H. Yan, Z. Lu, K. J. Griffith, J. Yan, G. Wang, H. Fan, J. Lu, W. Huang, B. Bao, X. Liu, C. Hou, Q. Zhang, Y. Li, J. Yu and H. Wang, *Nat. Commun.*, 2018, **9**, 4798.
3 J. Mu, G. Wang, H. Yan, H. Li, X. Wang, E. Gao, C. Hou, A. T. C. Pham, L. Wu, Q. Zhang, Y. Li, Z. Xu, Y. Guo, E. Reichmanis, H. Wang and M. Zhu, *Nat. Commun.*, 2018, **9**, 590.
4 G. M. Whitesides, *Angew. Chem., Int. Ed.*, 2018, **57**, 4258–4273.
5 H. Wang, M. Totaro and L. Beccai, *Adv. Sci.*, 2018, **5**, 1800541.
6 C. C. Kim, H. H. Lee, K. H. Oh and J. Y. Sun, *Science*, 2016, **353**, 682–687.
7 G. Wang, W. Huang, N. D. Eastham, S. Fabiano, E. F. Manley, L. Zeng, B. Wang, X. Zhang, Z. Chen, R. Li, R. P. H. Chang, L. X. Chen, M. J. Bedzyk, F. S. Melkonyan, A. Facchetti and T. J. Marks, *Proc. Natl. Acad. Sci. U. S. A.*, 2017, **114**, E10066–E10073.
8 L. Wang, D. Chen, K. Jiang and G. Shen, *Chem. Soc. Rev.*, 2017, **46**, 6764–6815.
9 H. R. Lee, C. C. Kim and J. Y. Sun, *Adv. Mater.*, 2018, **30**, 1–15.
10 S. Park, S. W. Heo, W. Lee, D. Inoue, Z. Jiang, K. Yu, H. Jinno, D. Hashizume, M. Sekino, T. Yokota, K. Fukuda, K. Tajima and T. Someya, *Nature*, 2018, **561**, 516–521.
11 C. Keplinger, J. Sun, C. C. Foo, P. Rothemund, G. M. Whitesides and Z. Suo, *Science*, 2013, **341**, 984.
12 C. Yang and Z. Suo, *Nat. Rev. Mater.*, 2018, **3**, 125–142.
13 J. Y. Sun, C. Keplinger, G. M. Whitesides and Z. Suo, *Adv. Mater.*, 2014, **26**, 7608–7614.
14 Z. Lei and P. Wu, *Nat. Commun.*, 2018, **9**, 1–7.
15 J. Kang, D. Son, G. J. N. Wang, Y. Liu, J. Lopez, Y. Kim, J. Y. Oh, T. Katsumata, J. Mun, Y. Lee, L. Jin, J. B. H. Tok and Z. Bao, *Adv. Mater.*, 2018, **30**, 1–8.
16 X. Pu, M. Liu, X. Chen, J. Sun, C. Du, Y. Zhang, J. Zhai, W. Hu and Z. L. Wang, *Sci. Adv.*, 2017, **3**, 1–11.
17 Y. Bai, B. Chen, F. Xiang, J. Zhou, H. Wang and Z. Suo, *Appl. Phys. Lett.*, 2014, **105**, 151903.
18 Q. Rong, W. Lei, L. Chen, Y. Yin, J. Zhou and M. Liu, *Angew. Chem., Int. Ed.*, 2017, **56**, 14159–14163.
19 F. Chen, D. Zhou, J. Wang, T. Li, X. Zhou, T. Gan, S. Handschuh-Wang and X. Zhou, *Angew. Chem., Int. Ed.*, 2018, **57**, 6568–6571.
20 Y. Ren, J. Guo, Z. Liu, Z. Sun, Y. Wu, L. Liu and F. Yan, *Sci. Adv.*, 2019, **5**, eaax0648.
21 Y. Ding, J. Zhang, L. Chang, X. Zhang, H. Liu and L. Jiang, *Adv. Mater.*, 2017, **29**, 1–7.
22 W. Qian, J. Texter and F. Yan, *Chem. Soc. Rev.*, 2017, **46**, 1124–1159.
23 B. Li, P. Jain, J. Ma, J. K. Smith, Z. Yuan, H. C. Hung, Y. He, X. Lin, K. Wu, J. Pfaendtner and S. Jiang, *Sci. Adv.*, 2019, **5**, eaaw9562.
24 L. D. Blackman, P. A. Gunatillake, P. Cass and K. E. S. Locock, *Chem. Soc. Rev.*, 2019, **48**, 757–770.
25 Y. Wang, T. Li, S. Li and J. Sun, *Chem. Mater.*, 2015, **27**, 8058–8065.

26 S. Bai, X. Li, R. Zhang, C. Li, K. Zhu, P. Sun, Y. Zhao, L. Ren and X. Yuan, *Chem. Eng. J.*, 2019, **357**, 667–677.
27 T. Zhou, X. Gao, B. Dong, N. Sun and L. Zheng, *J. Mater. Chem. A*, 2016, **4**, 1112–1118.
28 X. P. Morelle, W. R. Illeperuma, K. Tian, R. Bai, Z. Suo and J. J. Vlassak, *Adv. Mater.*, 2018, **30**, 1801541.
29 X. F. Zhang, X. Ma, T. Hou, K. Guo, J. Yin, Z. Wang, L. Shu, M. He and J. Yao, *Angew. Chem., Int. Ed.*, 2019, **58**, 7366–7370.
30 D. E. Mitchell, A. E. R. Fayter, R. C. Deller, M. Hasan, J. Gutierrez-Marcos and M. I. Gibson, *Mater. Horiz.*, 2019, **6**, 364–368.
31 Z. Zhang and X. Y. Liu, *Chem. Soc. Rev.*, 2018, **47**, 7116–7139.
32 C. I. Biggs, T. L. Bailey, B. Graham, C. Stubbs, A. Fayter and M. I. Gibson, *Nat. Commun.*, 2017, **8**, 1–11.
33 C. Wang, C. G. Wiener, P. I. Sepulveda-Medina, C. Ye, D. S. Simmons, R. Li, M. Fukuto, R. A. Weiss and B. D. Vogt, *Chem. Mater.*, 2019, **31**, 135–145.
34 D. England, F. Yan and J. Texter, *Langmuir*, 2013, **29**, 12013–12024.
35 Q. Shao and S. Jiang, *Adv. Mater.*, 2015, **27**, 15–26.
36 J. Wu, W. Lin, Z. Wang, S. Chen and Y. Chang, *Langmuir*, 2012, **28**, 7436–7441.
37 Y. He, Q. Shao, H. K. Tsao, S. Chen, W. A. Goddard and S. Jiang, *J. Phys. Chem. B*, 2011, **115**, 11575–11580.
38 J. Wu, W. Lin, Z. Wang, S. Chen and Y. Chang, *Langmuir*, 2012, **28**, 7436–7441.
39 X. Hou, Z. Wang, Z. Zheng, J. Guo, Z. Sun and F. Yan, *ACS Appl. Mater. Interfaces*, 2019, **11**, 20417–20424.
40 Y. Sun, Y. Y. Ren, Q. Li, R. W. Shi, Y. Hu, J. N. Guo, Z. Sun and F. Yan, *Chin. J. Polym. Sci.*, 2019, **37**, 1053–1059.
41 K. Parida, V. Kumar, W. Jiangxin, V. Bhavanasi, R. Bendi and P. S. Lee, *Adv. Mater.*, 2017, **29**, 1–8.
42 F. Fan and J. Szpunar, *Macromol. Mater. Eng.*, 2015, **300**, 99–106.
43 R. Li, Y. Si, Z. Zhu, Y. Guo, Y. Zhang, N. Pan, G. Sun and T. Pan, *Adv. Mater.*, 2017, **29**, 1–8.
44 Z. Qiu, Y. Wan, W. Zhou, J. Yang, J. Yang, J. Huang, J. Zhang, Q. Liu, S. Huang, N. Bai, Z. Wu, W. Hong, H. Wang and C. F. Guo, *Adv. Funct. Mater.*, 2018, **28**, 1–9.
45 J. Wu, Z. Wu, S. Han, B. R. Yang, X. Gui, K. Tao, C. Liu, J. Miao and L. K. Norford, *ACS Appl. Mater. Interfaces*, 2019, **11**, 2364–2373.
46 R. L. Truby, M. Wehner, A. K. Grosskopf, D. M. Vogt, S. G. M. Uzel, R. J. Wood and J. A. Lewis, *Adv. Mater.*, 2018, **30**, 1–8.
47 Z. Yuan, T. Zhou, Y. Yin, R. Cao, C. Li and Z. L. Wang, *ACS Nano*, 2017, **11**, 8364–8369.
48 Y. C. Lai, J. Deng, S. L. Zhang, S. Niu, H. Guo and Z. L. Wang, *Adv. Funct. Mater.*, 2017, **27**, 1–10.
49 C. X. Lu, C. B. Han, G. Q. Gu, J. Chen, Z. W. Yang, T. Jiang, C. He and Z. L. Wang, *Adv. Eng. Mater.*, 2017, **19**, 1–8.
50 Z. L. Wang, *ACS Nano*, 2013, **7**, 9533–9557.